ACSNANO
www.acsnano.org
ARTICLE

Design of a Photoactive Hybrid Bilayer Dielectric for Flexible Nonvolatile Organic Memory Transistors

Hongliang Chen,[†] Nongyi Cheng,[†] Wei Ma,[‡] Mingliang Li,[†] Shuxin Hu,[‡] Lin Gu,[‡] Sheng Meng,[‡] and Xuefeng Guo*[,†,§]

[†]Center for Nanochemistry, Beijing National Laboratory for Molecular Sciences, State Key Laboratory for Structural Chemistry of Unstable and Stable Species, College of Chemistry and Molecular Engineering, Peking University, Beijing 100871, People's Republic of China

[‡]Institute of Physics, Chinese Academy of Sciences, Beijing 100190, People's Republic of China

[§]Department of Materials Science and Engineering, College of Engineering, Peking University, Beijing 100871, People's Republic of China

Supporting Information

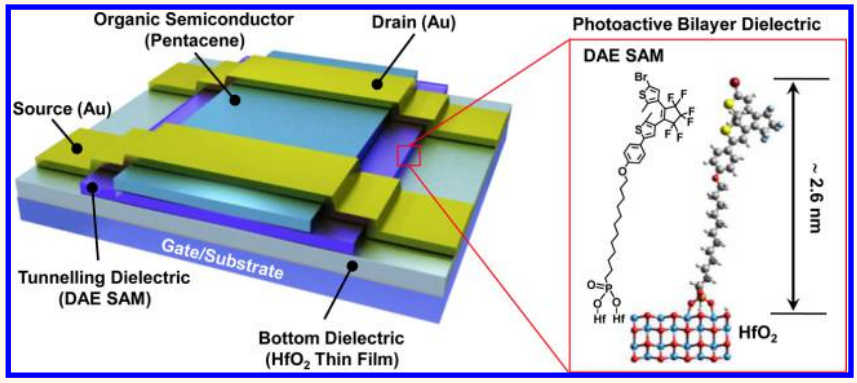

ABSTRACT: **Organic field-effect transistors (OFETs) featuring a photoactive hybrid bilayer dielectric (PHBD) that comprises a self-assembled monolayer (SAM) of photochromic diarylethenes (DAEs) and an ultrathin solution-processed hafnium oxide layer are described here. We photoengineer the energy levels of DAE SAMs to facilitate the charging and discharging of the interface of the two dielectrics, thus yielding an OFET that functions as a nonvolatile memory device. The transistors use light signals for programming and electrical signals for erasing (≤3 V) to produce a large, reversible threshold-voltage shift with long retention times and good nondestructive signal processing ability. The memory effect can be exercised by more than 10^4 memory cycles. Furthermore, these memory cells have demonstrated the capacity to be arrayed into a photosensor matrix on flexible plastic substrates to detect the spatial distribution of a confined light and then store the analog sensor input as a two-dimensional image with high precision over a long period of time.**

KEYWORDS: *organic field-effect transistor, flexible nonvolatile memory, diarylethene, self-assembled monolayer, photoactive hybrid dielectric*

Organic field-effect transistors (OFETs) are the basic building blocks for logic circuits that can be fabricated using low-cost techniques to produce large-area, lightweight, mechanically flexible arrays.[1,2] The advantageous properties of OFETs make them viable candidates for commercialization.[3−7] However, an OFET is usually volatile, meaning that once the gate voltage is removed, the device returns to the original OFF state. For OFETs to function as a nonvolatile organic memory transistor (OMT), alternative designs and mechanistic insights are in great need to improve their retention time, operational voltage, fatigue resistance, and integratability.[8−11]

In general, nonvolatile memories can be classified into three basic types, depending on their adopted architectures: capacitor, resistor, and transistor-based memories, as well as various combinations.[10] The capacitor-based memory is vulnerable to lose the stored data because the medium between

Received: August 24, 2015
Accepted: December 16, 2015
Published: December 17, 2015

DOI: 10.1021/acsnano.5b05313
ACS Nano 2016, 10, 436−445

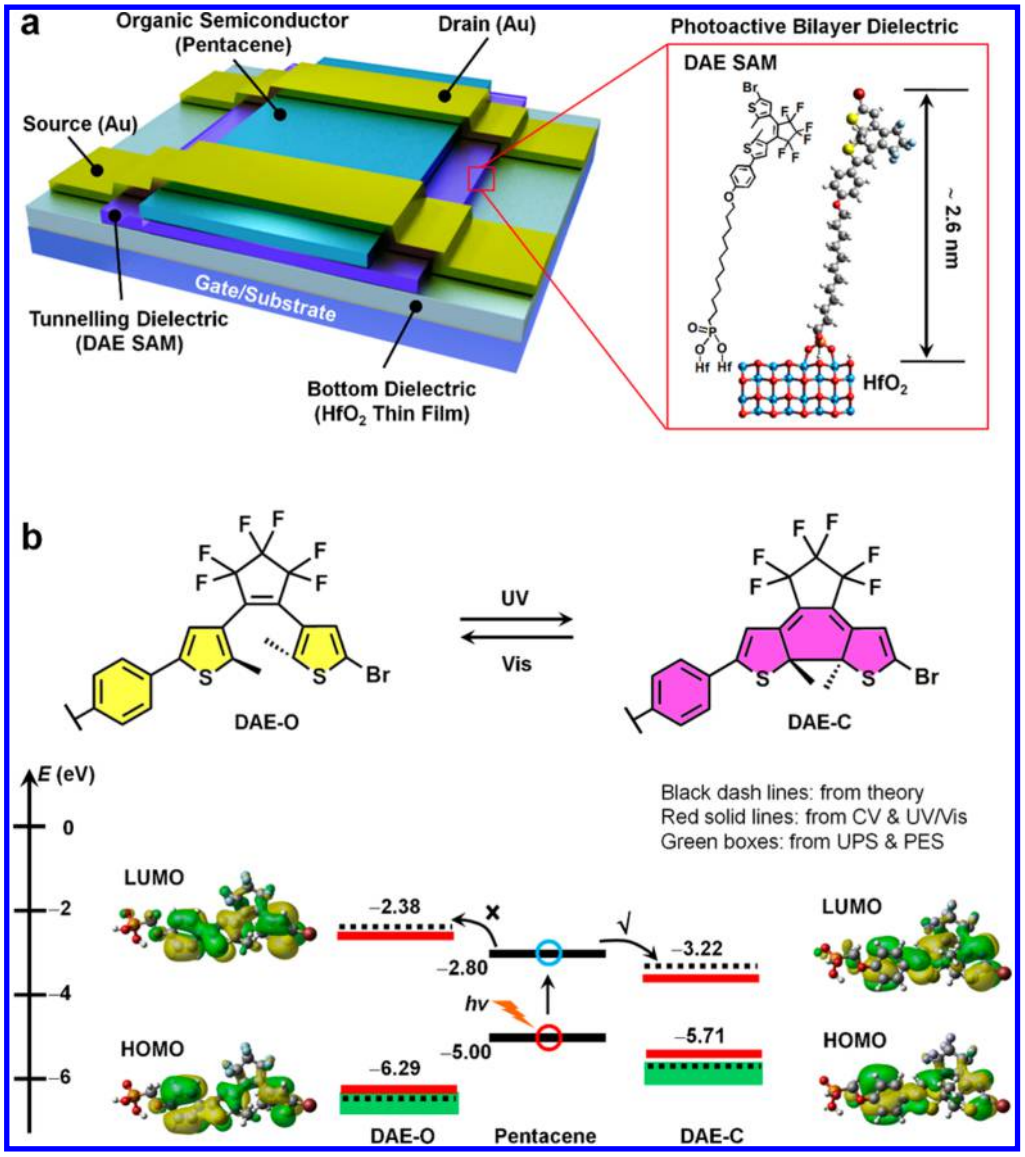

Figure 1. Device structure. (a) Schematic cross section of a PHBD OMT. The inset shows the molecular structure and a real-space model of a DAE bonding to the HfO_2 (110) surface through two Hf−O−P ligations and a hydrogen bond with the lowest adsorption energy (approximately 1.21 eV). (b) Energy level diagram of DAE-O and DAE-C. These values were obtained from DFT calculations, CV, UV−vis absorptions, UPS, and PES measurements. To clearly show the molecular orbitals, we omitted the long alkyl side chains. UV = ultraviolet (λ = 365 nm); vis = visible ($\lambda \geq$ 420 nm).

the electrodes is merely dielectric with nothing to stabilize the programmed state.[12] The organic resistive memory devices consist of organic-resistive layers between two electrodes, which typically act as either electrically insulating components or electrically conducting components under appropriate voltage conditions.[12] From the perspective of device fabrication, their advantages include simple device structures, low fabrication costs, and maximized storage density. However, the organic resistive memory devices require transistors for addressing signals in two-dimensional memory arrays because they do not possess third electrodes for signal addressing.[13] The third memory architecture that can be adopted is termed as OFET-based memory devices. Such transistor-based memories are appealing since they allow direct integration of the memory element within the standard device structures used in complementary integrated circuits.

To create memory effects in an OFET device, an electric field is required to generate independently stable states so that information can be encoded as "0" and "1" in the same transistor. The key to the electrical bistability in OMTs is charge trap engineering, which is similar to that of the traditional floating gate memory.[14,15] In general, nonvolatile OMTs reported to date create trap sites mainly using either an extra layer of metal and dielectric as a floating gate[16−22] or multilayer dielectrics,[23,24] both of which have the ability to store injected charges in the floating gate or at the dielectric interface upon application of the gate voltage. These stored charges function as an additional electric field to modulate the charge distribution in the conductive channel, thus resulting in the electrical bistability.[8−11] In both cases, both the programming signal and readout are typically based on the electrical processes. There is always a problem of storing recorded information in a memory device because the stored data can easily be retrieved by applying a voltage bias. To keep the data more reliable and read them nondestructively, ideally digital commuting between different signals without mutual interfer-

DOI: 10.1021/acsnano.5b05313
ACS Nano 2016, 10, 436−445

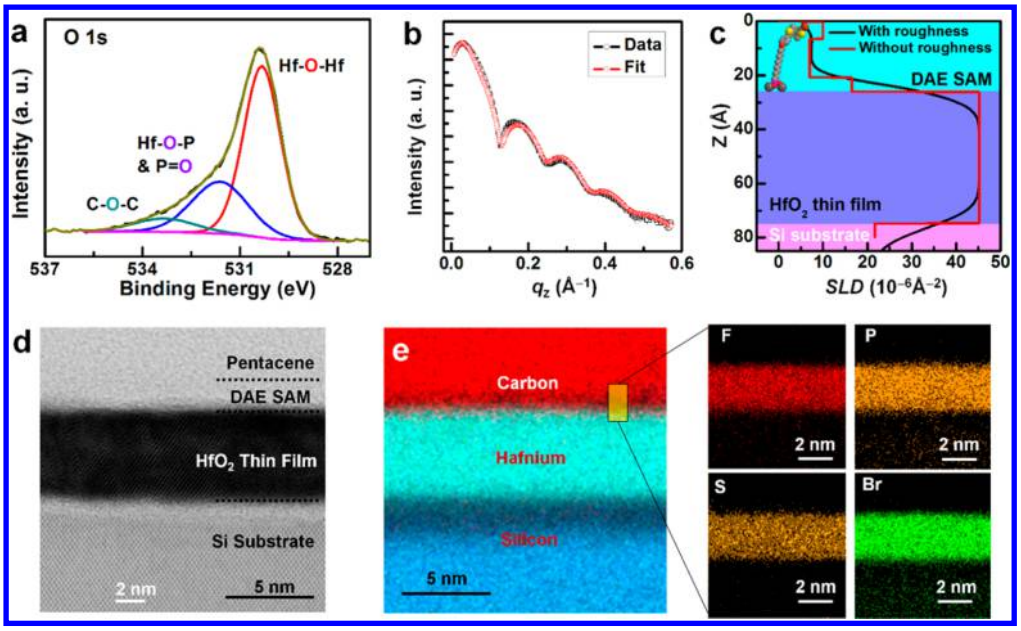

Figure 2. Characterization of the DAE/HfO_2 interface. (a) High-resolution XPS for O 1s. (b) XRR measurement (dark) of the SAM with a HfO_2 thin film on a silicon substrate and the corresponding fit (red). (c) *SLD* profile with (dark) and without (red) roughness. (d) Cross-sectional STEM image of a layer structure. The sample was prepared using a focused ion beam and imaged by STEM (200 kV). (e) Analyses of the elemental compositions of the SAM by means of an EDX system including carbon, hafnium, silicon, fluorine, phosphorus, sulfur, and bromine.

ence, such as optical and electric signals, is highly desirable. This is also useful to find practical application as a digital interface between optical and electric signals.[25] Another challenge of these OMTs is that the coercive erasing voltage required to detrap carriers from the trap sites increases with the decrease of the dielectric thickness, thus limiting the realization of large memory window with programming and erasing voltages less than 10 V. In some cases,[4] the utility of thin high-*k* AlO_x materials with a self-assembled monolayer remarkably reduced the programming voltage (below 10 V). However, the formation of AlO_x thin films needs complex fabrication processes, such as atomic layer deposition, thermal evaporation, and oxygen plasma treatment.

To achieve both the electrical bistability and nondestructive signal processing, a promising approach recently developed relies on the use of molecular photochromics because they undergo reversible photoisomerization between two isomers upon irradiation with light of different wavelengths.[26] These conformational changes result in remarkable differences in their electronic structures and in their distinct photophysical properties, thus forming the basis for new types of optoelectronic devices and molecular switches.[27] There are only few examples of photochromics-based OMTs[28−36] that were built on rigid substrates with thick dielectrics (200−300 nm) and required large erasing voltages to operate (>40 V). None of these photochromics-based OMTs have been integrated into memory arrays. Reducing the erasing voltages and demonstrating low-cost, large-area memory arrays on flexible substrates with high yield and good uniformity necessitate the development of a thin, defect-free dielectric that is solution-processable and readily integratable with standard transistors. Moreover, two challenging issues that are prerequisites for practical applications are to improve the stability of each state (retention ability) and the rewriting ability (fatigue resistance). Comparing different classes of molecular photochromics,[27] the diarylethene (DAE) family is superior because it provides the best fatigue resistance and good thermal stability of the two isomers. More importantly, both isomers exhibit very different electronic structures. Large changes in the frontier energy levels (highest occupied molecular orbit [HOMO] and lowest unoccupied molecular orbit [LUMO]) originate from changes in the π-conjugations. These unique characteristics have been applied to optically modulate charge carrier injection and thus the transport properties in DAE-hybridized devices.[27] In conjunction with recent theoretical calculations,[37] these experimental studies[38−40] suggest that a memory effect can be obtained by optically tuning the energy level alignments at the organic semiconductor/DAE interfaces. Therefore, by utilizing the tunability of the chemophysical properties of both DAE self-assembled monolayers (SAMs) and solution-processed high-*k* metal oxide thin dielectrics, in this work, we realized high-density arrays of low-voltage, nondestructive, and rewritable organic nonvolatile memory cells with high-precision imaging capability and long retention times on flexible plastic substrates, using a new type of OFETs featuring a photoactive hybrid bilayer dielectric (PHBD).

RESULTS AND DISCUSSION

Device Structure. The schematic cross section of the individual transistor architecture on heavily doped Si substrates is shown in Figure 1a. The PHBD is composed of an ultrathin HfO_2 bottom dielectric and a DAE SAM tunneling dielectric (Figure 1a inset). The semiconductor is a 40 nm thick layer of pentacene. Taking into account the orbital energy levels of pentacene (approximately −5.00 eV for the HOMO and −2.80 eV for the LUMO), we computationally screened DAE molecules (terminated by a phosphonic acid group designed for self-assembly[41]) that feature different energy levels in their open (DAE-O) and closed (DAE-C) states. According to density functional theory (DFT) calculations (details can be found in the Supporting Information (SI, section 4), the molecular LUMO energy level was −2.38 eV, which is much

DOI: 10.1021/acsnano.5b05313
ACS Nano 2016, 10, 436−445

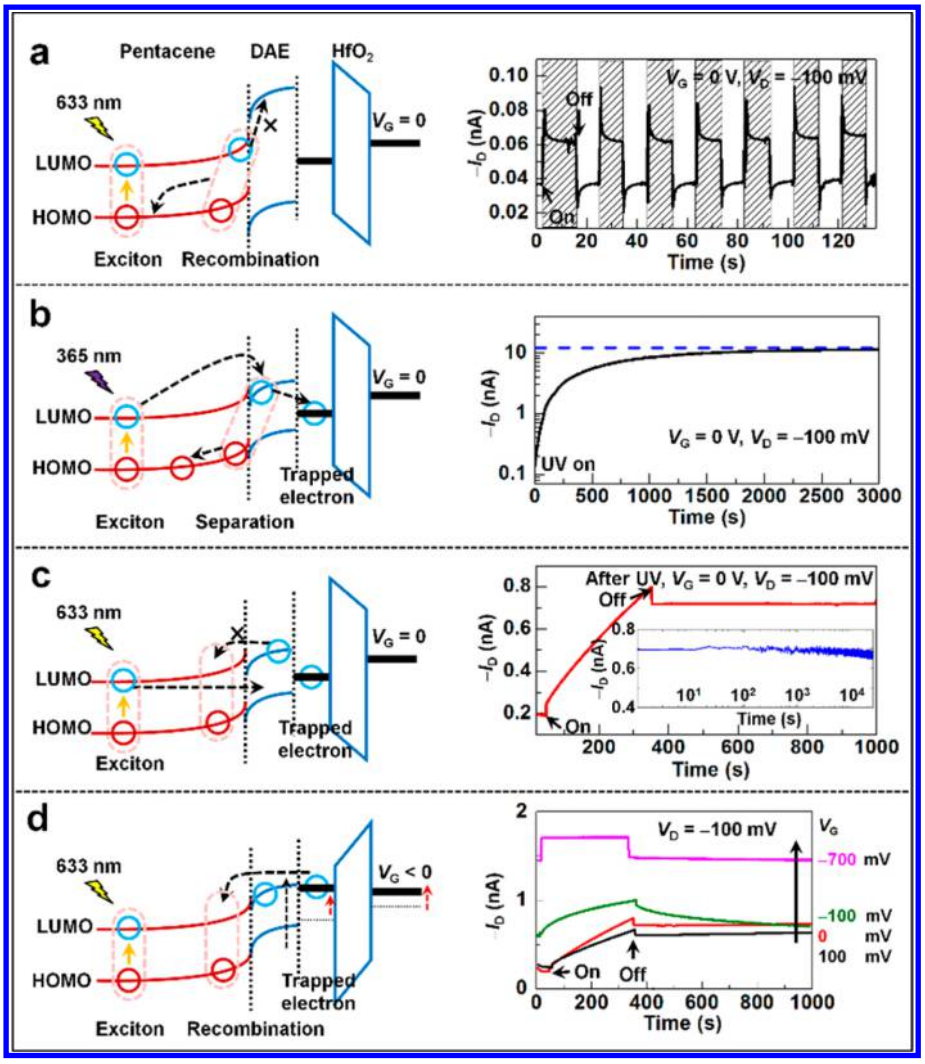

Figure 3. Mechanism demonstrations of nonvolatile memory effects. (a–d) Photocurrent generation mechanisms (left) and device photoresponses (right) under different conditions: (a, prior to UV illumination, V_D = −100 mV and V_G = 0; b, during UV illumination (365 nm, approximately 100 μW cm^{-2}), V_D = −100 mV and V_G = 0; c, visible light illumination (633 nm, 0.6 mW cm^{-2}) after UV irradiation for 600 s, V_D = −100 mV and V_G = 0; d, at variable V_G (100, 0, −100, and −700 mV) after UV irradiation for 600 s, V_D = −100 mV). The inset in panel c (right) shows the nondestructive readout over 3 h of continuous measurements with no information loss.

higher than that of pentacene (approximately −2.80 eV), with a band gap of approximately 3.91 eV. These values are consistent with cyclic voltammetry (CV) and UV–vis absorption measurements in thin films (Figure S1). Upon exposure to UV light (λ = 365 nm), the DAE molecule transformed from DAE-O to DAE-C through the formation of a C–C bond (Figure 1b), leading to π-electron delocalization. Importantly, this transformation significantly decreased the LUMO energy of DAEs to −3.22 eV (as well as the band gap to approximately 2.49 eV), which is lower than that of pentacene. The reverse process used visible light irradiation to recover the original high LUMO energy. Further UV photoelectron spectroscopy (UPS) and photoelectron spectroscopy (PES) on indium tin oxide (ITO) substrates (Figure S2) provided HOMO energy levels of −6.30 and −5.75 eV for DAE-O and DAE-C in solid films, respectively. These values are in good agreement with the values obtained from CV in thin films. The energy level diagram of DAE-O and DAE-C with respect to pentacene is schematically shown in Figure 1b and Table S1.

The molecular synthesis, HfO_2 thin film preparation, and device fabrication are detailed in the SI (sections 1, 2, and 3.1–3.2, Figures S3 and S4). From high-resolution X-ray photoelectron spectroscopic (XPS) studies, we found that the O 1s signals of DAE SAMs (Figure 2a) could be fit with three components: 530.3, 531.6, and 533.4 eV. These data can be assigned to Hf–O–Hf, Hf–O–P (or P═O of the phosphonate group), and C–O–C, respectively.[42] In combination with the appearance of new transitions from P, Br, F, and S (Figures S5 and S6), these results reveal the successful attachment of DAE molecules on the HfO_2 surface. Furthermore, the DAE films are very stable; no oxidized sulfur atoms were observed after exposure to UV light (λ = 365 nm, ~100 μW cm^{-2}) for 30 min (Figure S6).[43] Low-angle X-ray reflectivity (XRR) was used to determine the PHBD structure and illustrate the formation of a SAM in a highly dense manner (Figure 2b and Figure S4). The scattering length density profile provided further evidence of the homogeneous assembly of the monolayer (Figure 2c), which could be modeled as a three-layer structure with different electron densities: a DAE layer (approximately 0.8 nm), an alkyl chain layer (approximately 1.5 nm), and a phosphate anchor layer (approximately 0.3 nm) (Table S2). This fit yielded a monolayer thickness of

DOI: 10.1021/acsnano.5b05313
ACS Nano 2016, 10, 436–445

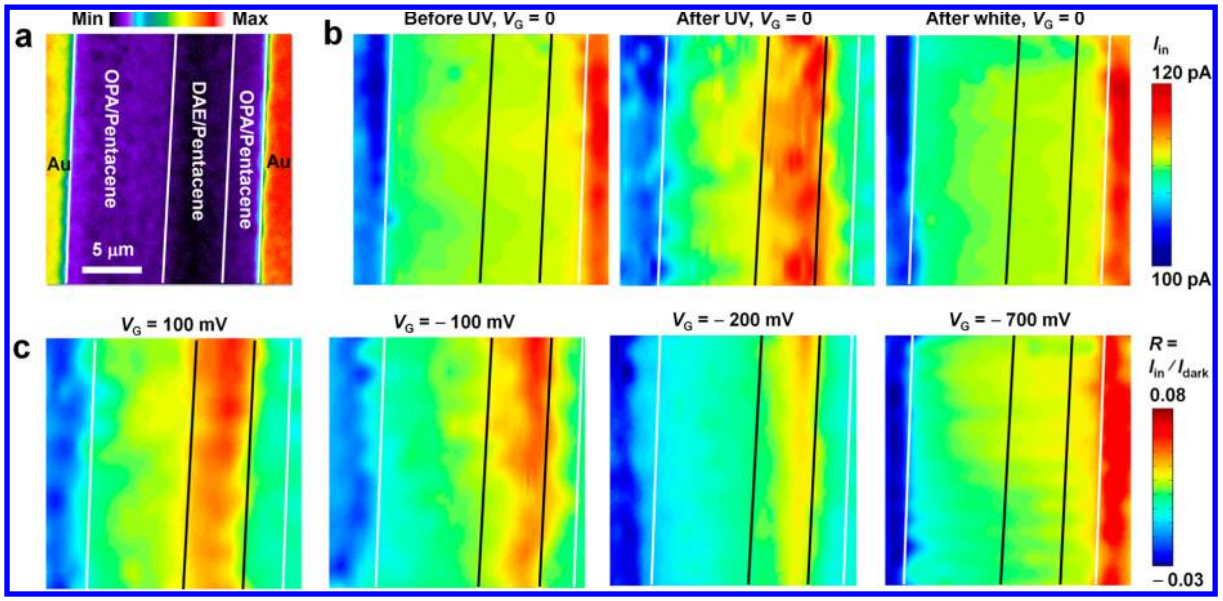

Figure 4. Scanning photocurrent images. (a) Fluorescent image of a mapping device showing a 5 μm wide DAE SAM ribbon in the middle of the channel. The scale bar applies to all panels. (b) Scanning current images prior to and after UV illumination (365 nm, approximately 100 μW cm^{-2}, 600 s), and after further white-light illumination (≥420 nm, 1.7 mW cm^{-2}, 600 s). V_D = −100 mV and V_G = 0. (c) Spatial maps of the read-current ratios ($R = I_{in}/I_{dark}$) for the same device taken after UV illumination for 600 s at V_D = −100 mV and variable V_G (100, −100, −200, and −700 mV). All of the current mappings were performed with a 633 nm laser light (excitation power, 90 μW; spot size, 1 μm).

approximately 2.6 nm, which was consistent with an optimized real-space model of DAEs stably bound to the HfO_2 surface in a tridentate bridging mode (two Hf−O−P ligations and an additional hydrogen bond) (Figure 1a inset and SI, section 4 and Figure S7). Figure 2d,e shows cross-sectional scanning transmission electron microscopic (STEM) images of the layered structure: silicon substrate/HfO_2 thin film/DAE SAM/pentacene. This visualization was realized using the double-spherical aberration-corrected STEM with a spatial resolution of *ca.* 0.80 Å. The elemental compositions of the individual layers were analyzed using an energy-dispersive X-ray system (EDX). The presence of F, P, S, and Br (Figure 2e inset) was the fingerprint of the molecules in the monolayer that confirmed the structure of the hybrid dielectrics as a combination of an HfO_2 thin film and a DAE SAM with a total thickness of approximately 7.7 nm. Solid-state UV/vis absorption spectroscopic studies (SI, section 3.3 and Figure S8) reveal that alternating illumination with UV and white light induced quantitative and reversible conversion between two distinct states,[44,45] thus setting the foundation for the following investigation of the device photoresponses.

Mechanism of Nonvolatile Memory Effects. After understanding the structure of the pentacene/DAE interface, we then focused on probing the photoresponsive behaviors of PHBD OMTs. The capacitance of the PHBD was approximately 0.50 μF/cm^2, measured using impedance spectroscopy (Figure S9). Typical output and transfer characteristics for a PHBD OMT are presented in Figure S10. All of the devices had stable operations in ambient air at low voltages (less than −3.0 V). The average mobility of 0.7 ± 0.08 cm^2 V^{-1} s^{-1} and the on/off ratio on the order of approximately 10^5 on silicon substrates were achieved based on more than 30 individual transistors on different wafers (SI, sections 3.1−3.2). Figure 3a−d shows the working mechanism and device photoresponses in the different states. Initially, we chose irradiation with 633 nm light (0.6 mW cm^{-2}) because the programming signal does not disturb the DAE conformation (nondestructive programming) (Figure S11). We observed a sudden source/drain current (I_D) jump as shown in Figure 3a (right). The current jump was attributed to the net photocurrent (I_n), suggesting that the memory cell was not working. The photoexcited electrons could not cross the barrier between the LUMOs of pentacene and DAE into the DAE/HfO_2 interface (Figure 3a left). UV light (365 nm) was required to preset the device so that it could function as a memory cell. UV irradiation caused both the isomerization from DAE-O to DAE-C and the creation of a photoexcited electron. As the DAE LUMO was lowered with respect to pentacene (Figure 3b left), the high-energy electrons could tunnel through the DAE SAM and charge the DAE/HfO_2 interface. To reveal these processes, we performed the real-time excited-state time-dependent density functional theory (TDDFT) simulations. It may include three processes: (i) intermolecular electron transfer from pentacene to DAE molecules with a lifetime of 324 fs (Figure S12a); (ii) intramolecular electron transfer in DAE (within 1 ps);[46] (iii) intermolecular electron transfer from DAE to HfO_2 semiconductor. As shown in Figure S12b, the energy difference between DAE and HfO_2 could drive the photoexcited electrons to transfer from DAE to the oxide interface. The third process is also very fast (with lifetime in the range from several femtoseconds to hundreds of femtoseconds).[47] Therefore, the total process happens within a picosecond and can be described as a tunneling process. These trapped electrons provide an additional negative electrical field, thus leading to an increase in the device currents (I_{in}) (Figure 3b right). This I_{in} includes two components: the net photocurrent (I_n) and the photocurrent induced by the charged DAE/HfO_2 interface (I_{ph}), that is, $I_{in} = I_n + I_{ph}$. After presetting the device, progressive nondestructive programming was realized by 633 nm visible light irradiation, as shown in Figure 3c (right). Remarkably, the device persisted in a high conductance state (I_{ph}) over a long retention time after the visible light was turned off. After over 3 h of continuous measurements in the dark, the devices still retained recorded information with no information loss (nondestructive readout)

DOI: 10.1021/acsnano.5b05313
ACS Nano 2016, 10, 436−445

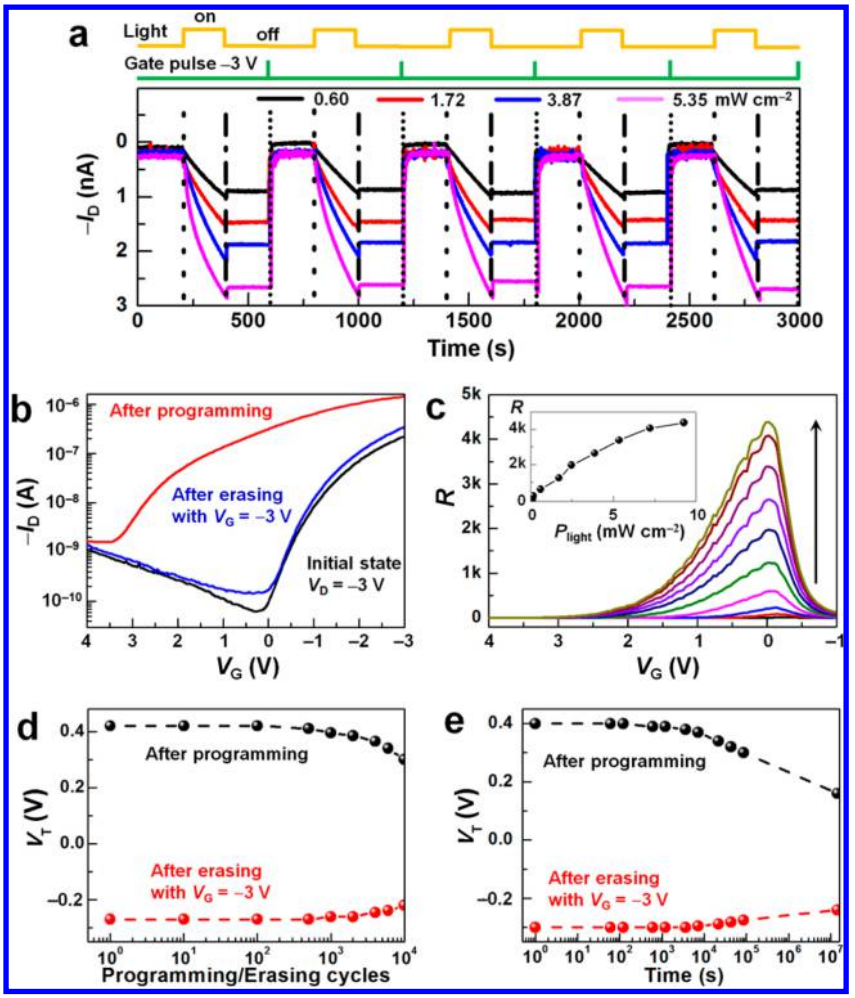

Figure 5. Memory characteristics of PHBD OMTs. (a) Five representative programming and erasing cycles of a device as a function of P_{light}. Programming: 633 nm light illumination (200 s) with four different intensities (0.60, 1.72, 3.87, and 5.35 mW cm^{-2}). Erasing: −3 V gate pulse (1 s); V_D = −100 mV and V_G = 0. (b) Large V_T window when V_G scanned from −3 to 4 V; V_D = −3 V. (c) Gate-dependent read-current ratios (R) as a function of P_{light}. The P_{light} of the 633 nm light ranged from 0, 0.10, 0.12, 0.17, 0.60, 1.72, 2.48, 3.87, 5.35, 7.22, to 9.27 mW cm^{-2}. The data were recorded by 200 s of illumination from its initial state for each intensity; V_D = −3 V. The inset shows the relationship between R and P_{light} at V_G = 0. (d) Fatigue resistance of PHBD OMTs at V_D = −1 V when V_G scanned from −1 to 1 V. After 10^3 cycles, the V_T window was larger than 0.7 V; after 10^4 cycles, the V_T window was still larger than 0.5 V. (e) Retention characteristics for PHBD OMTs at V_D = −1 V when V_G scanned from −1 to 1 V. After over 7 days, the device still had a measurable V_T window (larger than 0.4 V). All of the devices were preset to an initial state by UV light illumination (365 nm, approximately 600 s) and a −3 V gate pulse (1 s). For panels b,d,e, programming was carried out with 633 nm light illumination (0.6 mW cm^{-2}, 600 s), while erasing was carried out with a −3 V gate pulse (1 s).

except for a slight noise increase (Figure 3c right). This result is reasonable because the LUMO energy of DAE-C is lower than that of pentacene, and the trapped electrons at the DAE/HfO_2 interface were efficiently prevented from leaking away through the pentacene/DAE interface (Figure 3c left). Along with the thermal stability of DAE-C, these results demonstrated the significant nonvolatile memory capability of these PHBD OMTs. White light illumination (≥420 nm) was used to recover the initial DAE-O isomer as well as the original electronic structure at the pentacene/DAE interface (data not shown), thus discharging the DAE/HfO_2 interface in addition to the voltage bias. Another important way to erase information is to apply a negative voltage from the back gate (V_G) (Figure 3d). We found that the devices showed a nonvolatile memory effect when $V_G \geq 0$, while their persistent current was not retained when $V_G < 0$. If V_G was as large as −700 mV, the devices only displayed photocurrents (Figure 3d right). This result can be explained by the following mechanism (Figure 3d left): the negative V_G raised the defect energy level of the dielectric interface as well as the LUMO energy of DAE-C, resulting in the continuous release of the trapped electrons from the DAE/HfO_2 interface. When the LUMO energy of DAE-C increased to higher than that of pentacene, the photogenerated electron−hole pairs could not be efficiently separated at the pentacene/DAE interface to charge the DAE/HfO_2 interface, similarly to the case of DAE-O (Figure 3a). Although both methods (white light and V_G) highlighted the resettability of the device, V_G was favored because it did not require resetting the devices for the next writing and reading cycle.

Scanning Photocurrent Mapping. To further verify the underlying physical mechanisms of the memory effect, we conducted spatially resolved scanning photocurrent mapping measurements. For comparison, we lithographically patterned the DAE SAM to a 5 μm wide ribbon positioned in the middle of the channel (Figure S13 and Figure 4a). The remaining part of the channel was modified with *n*-octadecylphosphonic acid (OPA). Figure 4b mapped the total current increase ($I_{in} = I_{light}$

DOI: 10.1021/acsnano.5b05313
ACS Nano 2016, 10, 436−445

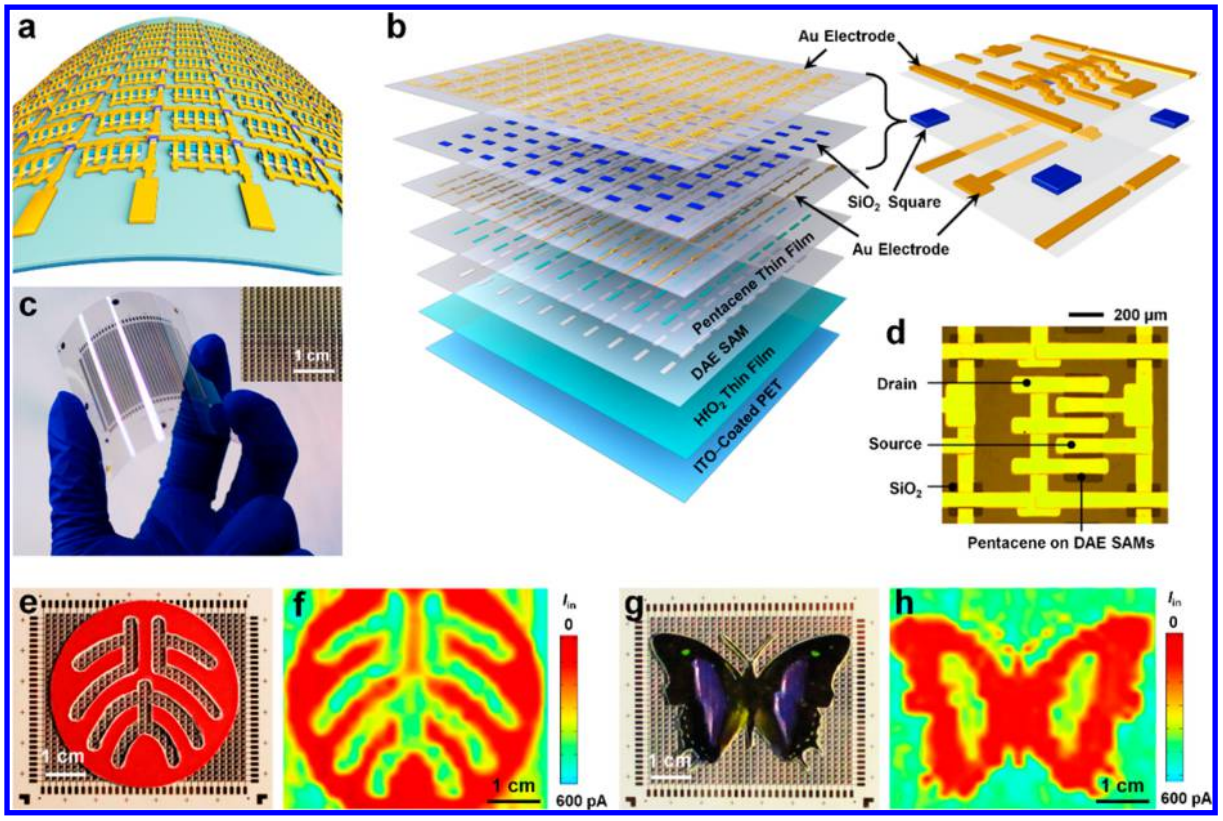

Figure 6. Flexible PHBD OMT arrays. (a) Schematic diagram of a sensor array. (b) Layered structures of a sensor array from bottom to top: ITO-coated PET, 5.1 nm thick HfO_2 thin film, 2.6 nm DAE SAM, 40 nm thick pentacene thin film, Au electrode, 100 nm thick SiO_2 square array, and Au electrode. The inset shows the magnified structure of the top three layers in one pixel. (c) Top-view photograph of a complete 30-by-30 sensor array on flexible substrates (effective area: 5 × 5 cm^2). The inset shows a magnified image of the array. (d) Detailed optical image of an individual pixel. (e–h) Top-view photographs and corresponding current mappings for two objects: a Peking University logo and a butterfly. UV light (365 nm) was used for resetting and programming; a gate pulse (−3 V) was used for erasing; V_D = −100 mV and V_G = 0.

$-I_{dark}$) at V_G = 0 and under a −100 mV source/drain bias (V_D) before UV illumination (DAE-O), after UV illumination (DAE-C), and after further white-light illumination (DAE-O). Note that the current changes appeared in five separate zones (from left to right: source, OPA/pentacene, DAE/pentacene, OPA/pentacene, and drain). Only in the DAE-C state did we observe a high-current region with a similar width to the DAE ribbons in the middle of the conducting channel, which confirmed that UV light or DAE-C is a prerequisite for efficient hot electron injection and trapping. Similarly, current mapping after UV irradiation was also carried out under a V_G fixed at 100, −100, −200, and −700 mV (Figure 4c). We observed the consistent progressive decrease of the read-current ratios ($R = I_{in}/I_{dark}$) with V_G varying from 100, −100, and −200 mV, and even the disappearance of R at V_G = −700 mV. These results demonstrated the gate-enforced charge detrapping mechanism of the PHBD and the erasability of stored information in the PHBD OMTs.

To further confirm the mechanism, we carried out two sets of control experiments where we built pentacene thin film transistors without DAE SAMs and the pure DAE SAM device without pentacene. In the first case, the devices did only show the photocurrent jumps both before and after UV light illumination (Figure S14). In the second case, we did not get any measurable current in pure DAE SAM-based devices because a DAE monolayer is insulating (data not shown). Another possibility for the switching mechanism is the variations in capacitance of DAE SAM−HfO_2 hybrid dielectrics. Control experiments demonstrated that neither UV nor visible light illuminations caused a capacitance change in the hybrid dielectrics (Figure S9). In conjunction with the theoretical calculations which show that there is a negligible difference in the molecular dipole moments for the two states (5.3 D for DAE-O and 5.6 D for DAE-C), these results preclude the effects of either capacitive coupling[28] or the built-in electric field (induced by the change of the dipole moment)[30] on the photoresponsive behavior described above.

Memory Characteristics of PHBD OMTs. Figure 5a shows the programming and erasing cycles of I_D as a function of light intensity (P_{light}). The device was first preset to an initial state by UV light illumination (approximately 600 s) and a−3 V gate pulse (1 s). For programming, 633 nm light with four different levels of P_{light} was applied to record information. After removing the light, the device retained the stored information over a long retention time (at least 3 h, Figure 3c). The stronger the input signal intensity, the higher the readout current. For erasure, a −3 V gate pulse was applied to discharge the DAE/HfO_2 interface and thus recover the initial current. The programming/erasing process was reversible, as shown by five representative cycles in Figure 5a. These results demonstrated the reproducibility and programmability of the nonvolatile memory capacity.

In addition to I_D, the threshold voltage (V_T), another feature of an OFET, is the second method to read information and evaluate the retention ability of a memory device. The exact V_T depends on the scanning voltage as well as the intensity and

DOI: 10.1021/acsnano.5b05313
ACS Nano 2016, 10, 436–445

duration of the programming light (Figure 5b and Figure S15). To read the maximum information, UV light illumination (approximately 600 s) followed by a −3 V gate pulse (1 s) was applied to the devices to preset their initial state. Then, V_T was examined by measuring I_D as a function of V_G during the programming/erasing process. For example, V_T significantly shifted from approximately 0 to 3.6 V when V_G scanned from −3 to 4 V (P_{light} = 0.6 mW cm^{-2} for 600 s) (Figure 5b), while V_T shifted from approximately −0.3 to 0.4 V when V_G scanned from −1 to 1 V (P_{light} = 0.6 mW cm^{-2} for 600 s) (Figure S15a). The memory window was found to be as large as 50% of the working voltage and was sufficient for reliable memory operations. On the basis of the data from Figure S15b, we calculated the read-current ratios (R) as a function of V_G and P_{light} (Figure 5c). We found that the R at each P_{light} reached a maximum at V_G = approximately 0 and increased to near saturation with increasing P_{light}, similarly to V_T (Figure S15). Significantly, the highest R value was as high as 4.4 × 10^4, 2 orders of magnitude higher than AlO_X/SAM hybrid dielectrics (10^2).[4]

To evaluate the fatigue resistance of PHBD OMTs, we applied 10^4 programming/erasing cycles to a device and monitored the associated V_T changes by scanning V_G from −1 to 1 V. As shown in Figure 5d, the device maintained the constant V_T window (approximately 0.7 V) without obvious degradation for up to 10^3 cycles. After that point, the device started to slowly degrade; the initial V_T could no longer be restored, and the V_T window narrowed. However, after 10^4 cycles, the V_T window was still larger than 0.5 V and allowed for a clear readout. This value is within 2 orders of magnitude of modern silicon-based floating-gate transistors widely used for flash memory (10^6 cycles).[48] Data retention is also of crucial importance for nonvolatile memory applications. Most OMTs suffer from charge loss during the readout operation. In our case, both the 633 nm light programming and electrical readout were nondestructive and did not induce a conformation transition or instability of the DAE SAMs. As previously demonstrated, the long retention time (approximately 3 h) was achieved by using I_D as the readout signal (Figure 3c). We found that using V_T as the readout signal could significantly improve the retention time. The results in Figure 5e show that the device still had a measurable V_T window (larger than 0.4 V) for unambiguous readouts after over 7 days of uninterrupted V_T monitoring. In fact, we preset a device *via* UV light irradiation and measured the initial V_T window to be approximately 0.65 V. The device still displayed a nearly similar V_T window (approximately 0.60 V) after being maintained in the dark for more than one-half of a year. These results suggested that the erasing voltage (−3 V) might be the major factor that caused device degradation. In general, the programming, erasing, and reading processes of conventional floating memories are based on the electrical processes that cause the obvious device degradation. Our light programming design opens up a solution to improve the retention time.

Flexible PHBD OMT Arrays. After comprehensively understanding the high-performance nonvolatile memory effect of individual OMTs, we then moved to demonstrate its integratability for potential imaging applications.[49,50] To do so, a flexible active-matrix sensor array with high density was fabricated. Figure 6a illustrates the schematic diagram of a nonvolatile PHBD OMT-based sensor array. The sensors were fabricated on ITO-coated polyethylene terephthalate (PET) sheets (Figure 6b). The detailed fabrication process is outlined in the Supporting Information. Figure 6c shows a top-view photograph of a complete 30-by-30 array with 900 memory cells arranged in a flexible transparent substrate (5 × 5 cm^2); a magnified view of one pixel is shown in Figure 6d. The devices showed an average mobility of approximately 0.03 ± 0.01 cm^2 V^{-1} s^{-1} and on/off ratio of approximately 10^4 when operated at a gate voltage as low as −3 V (Figure S16). This bendable active-matrix sensor array, which can endure harsh physical stresses (SI, section 3.4, Figures S17−S19), enabled us to measure the spatial distribution of the incident light applied to it and to store the two-dimensional analogue image for more than 1 week after the visible light was turned off. Figure 6e−h demonstrates the imaging capability of the sensor array. UV light was used for resetting and programming, and a gate pulse was used for erasing. The lights were applied in the shapes of two matters: a Peking University logo and a butterfly. We first imaged the logo of Peking University by UV light irradiation (365 nm, 100 μW cm^{-2}, 200 s). As seen in Figure S20, the current distribution of the programmed cells and the background were mainly located at approximately 450 and 50 pA, respectively, and the contrast between them showed a clear shape for up to 24 h after removing the light and electric voltages (Figure 6f). Notably, the sensor array can be programmed repeatedly after erasing the stored information with a gate pulse (−3 V, 1 s) so that the spatial distribution of the applied light was successfully recovered. Good contrast for the butterfly image was still achieved by recycling the same sensor array (Figure 6g,h), demonstrating the imaging capability with high precision and resettability.

CONCLUSION

This work presented a general approach for developing highly integrated, cost-effective, transparent, and functional flexible electronics that are controllable on large areas, using high-performance OFETs with desired functionalities as the building blocks. By sophisticatedly designing and fabricating a unique PHBD OMT featuring solution-processed ultrathin hybrid dielectrics on flexible plastic substrates, we realized a high-density, foldable, lightweight nonvolatile OMT array that worked at low operation voltages (≤3 V) to produce a large, reversible threshold-voltage shift with long retention times (half a year) and >10^4 memory cycles in an invasive manner. More importantly, these active-matrix sensor arrays demonstrated the capacity to record the spatial distribution of the confined light and then image the two-dimensional matters with high precision and resettability. The universality of this technology and the compatibility of organic electronics with flexible substrates, in combination with the proved device's reproducibility, sensing ability, and endurance of harsh physical stresses, suggest a feasible route toward their implementation for future practical applications, including health care and tissue detection, sensors, displays, solar cells, smart skin, environmental monitoring, and consumer electronic appliances.

METHODS

Hafnium Oxide Thin Film Preparation. The sol−gel process to prepare hafnium oxide dielectric can be found in ref 41. Heavily doped n-type silicon wafers (KMT Corporation) after removing the SiO_2 layer on the surface were cleaned in a Piranha solution (volume ratio of components: H_2SO_4/H_2O_2 = 70:30) by heating at 110 °C for 2 h, followed by rinsing thoroughly with the deionized (DI) water, sonicated for 15 min in a RCA solution (volume ratio of components: DI water/ammonium hydroxide/H_2O_2 = 5:1:1), rinsed and dried

DOI: 10.1021/acsnano.5b05313
ACS Nano 2016, 10, 436−445

under a nitrogen gas, and used immediately. A hafnium oxide sol–gel solution was prepared by dissolving hafnium(IV) chloride ($HfCl_4$) (99.9% Alfa Aesar) in ethanol (distilled and deoxygenated by argon before use) in a glovebox (argon atmosphere), followed by adding a mixture of nitric acid (HNO_3) and DI water in air (molar ratio of components: $HfCl_4$/EtOH/HNO_3/H_2O = 1:410:5:5). The solution was filtered using a 0.2 μm PTFE syringe filter and heated at 50 °C for 3 h to promote hydrolysis and polymerization of HfO_2 sol–gel. Hafnium oxide films were prepared by spin-coating the HfO_2 sol–gel solutions onto the cleaned Si substrates at 6000 rpm for 30 s. After hydrolyzation in air for 1 h, the films were annealed in an oven at 600 °C for 30 min in air, then removed and cooled to the room temperature.

HfO_2 films prepared on flexible substrates were performed as followed:[51,52] A hafnium oxide sol–gel solution was prepared by the same method as mentioned above. HfO_2 films were prepared by spin-coating the sol–gel solution onto a cleaned ITO-coated PET substrate (Sigma-Aldrich, $L \times W \times$ thickness: 1 ft × 1 ft × 5 mil) in two steps of 1000 rpm for 3 s and 3000 rpm for 30 s. After being hydrolyzed in air for 1 h, the films were exposed to UV/O_3 at 200 °C for 30 min, then removed and cooled to the room temperature.

Memory Cell Fabrication. After the formation of hafnium oxide dielectric, silicon substrates were immediately immersed into a solution of 0.1 mM DAE in THF/ethanol (1:1) for 24 h at room temperature in an argon atmosphere for preparing DAE SAMs. Then, a 40 nm thick pentacene (TCI, purified by sublimation) was deposited as a semiconductor layer at a rate of 0.1 Å/s under a pressure of 5×10^{-4} Pa. The gold source and drain contacts (40 nm) were vacuum-deposited on the semiconductor layer through a shadow mask. The channel length (L) and width (W) were 100 and 1000 μm, respectively.

Flexible Memory Array Fabrication. For flexible sensor arrays on PET substrates, the self-assembly process of forming DAE SAMs was the same as that on silicon substrates. On top of the DAE monolayer, a 40 nm thick layer of pentacene (TCI, purified by sublimation) was deposited by vacuum sublimation through a shadow mask. Then, interdigitated metal contacts (Au, 40 nm) were formed on top of pentacene by thermal evaporation through different shadow masks with designed patterns in two steps. The channel length (L) and width (W) were 120 and 800 μm, respectively. To insulate source and drain contacts at the crossing section, a 100 nm thick layer of a SiO_2 square array were deposited by electron beam thermal evaporation through a shadow mask before the second step of metal electrode depositions. The control gates of all 900 memory cells were connected to the bottom surface, and the ITO layer was used as the global back gate. More information about molecular synthesis, device characterization, theoretical calculation, and supplementary data can be found in the Supporting Information.

ASSOCIATED CONTENT

Supporting Information

The Supporting Information is available free of charge on the ACS Publications website at DOI: 10.1021/acsnano.5b05313.

Additional figures and tables showing molecular synthesis, general methods, details of device fabrication, theoretical calculation, and additional references (PDF)

AUTHOR INFORMATION

Corresponding Author

*E-mail: guoxf@pku.edu.cn.

Notes

The authors declare no competing financial interest.

ACKNOWLEDGMENTS

The authors thank Prof. Colin Nuckolls very much for enlightening discussions. This work was supported by the 973 Project (2012CB921404) and the National Natural Science Funds of China (21225311, 91333102, and 21373014).

REFERENCES

(1) Wang, C.; Dong, H.; Hu, W.; Liu, Y.; Zhu, D. Semiconducting π-Conjugated Systems in Field-Effect Transistors: A Material Odyssey of Organic Electronics. *Chem. Rev.* **2012**, *112*, 2208–2267.

(2) Sokolov, A. N.; Tee, B. C. K; Bettinger, C. J.; Tok, J. B. H; Bao, Z. Chemical and Engineering Approaches to Enable Organic Field-Effect Transistors for Electronic Skin Applications. *Acc. Chem. Res.* **2012**, *45*, 361–371.

(3) Klauk, H.; Zschieschang, U.; Pflaum, J.; Halik, M. Ultralow-Power Organic Complementary Circuits. *Nature* **2007**, *445*, 745–748.

(4) Sekitani, T.; Yokota, T.; Zschieschang, U.; Klauk, H.; Bauer, S.; Takeuchi, K.; Takamiya, M.; Sakurai, T.; Someya, T. Organic Nonvolatile Memory Transistors for Flexible Sensor Arrays. *Science* **2009**, *326*, 1516–1519.

(5) Noh, Y. Y.; Zhao, N.; Caironi, M.; Sirringhaus, H. Downscaling of Self-Aligned, All-Printed Polymer Thin-Film Transistors. *Nat. Nanotechnol.* **2007**, *2*, 784–789.

(6) Smits, E. C. P.; Mathijssen, S. G. J.; van Hal, P. A.; Setayesh, S.; Geuns, T. C. T.; Mutsaers, K. A. H. A.; Cantatore, E.; Wondergem, H. J.; Werzer, O.; Resel, R.; et al. Bottom-Up Organic Interrated Circuits. *Nature* **2008**, *455*, 956–959.

(7) Crone, B.; Dodabalapur, A.; Lin, Y.-Y.; Filas, R. W.; Bao, Z.; LaDuca, A.; Sarpeshkar, R.; Katz, H. E.; Li, W. Large-Scale Complementary Integrated Circuits Based on Organic Transistors. *Nature* **2000**, *403*, 521–523.

(8) Dhar, B. M.; Özgün, R.; Dawidczyk, T.; Andreou, A.; Katz, H. E. Threshold Voltage Shifting for Memory and Tuning in Printed Transistor Circuits. *Mater. Sci. Eng., R* **2011**, *72*, 49–80.

(9) Guo, Y.; Yu, G.; Liu, Y. Functional Organic Field-Effect Transistors. *Adv. Mater.* **2010**, *22*, 4427–4447.

(10) Han, S. T.; Zhou, Y.; Roy, V. A. L. Towards the Development of Flexible Non-Volatile Memories. *Adv. Mater.* **2013**, *25*, 5425–5449.

(11) Leong, W. L.; Mathews, N.; Tan, B.; Vaidyanathan, S.; Dotz, F.; Mhaisalkar, S. Towards Printable Organic Thin Film Transistor Based Flash Memory Devices. *J. Mater. Chem.* **2011**, *21*, 5203–5214.

(12) Scott, J. C.; Bozano, L. D. Nonvolatile Memory Elements Based on Organic Materials. *Adv. Mater.* **2007**, *19*, 1452–1463.

(13) Cho, B.; Song, S.; Ji, Y.; Kim, T.-W.; Lee, T. Organic Resistive Memory Devices: Performance Enhancement, Integration, and Advanced Architectures. *Adv. Funct. Mater.* **2011**, *21*, 2806–2829.

(14) Sze, S. M. *Physics of Semiconductor Devices*; Wiley-VCH, 1989.

(15) Kahng, D.; Sze, S. M. A Floating Gate and Its Application to Memory Devices. *Bell Syst. Tech. J.* **1967**, *46*, 1288–1295.

(16) Mushrush, M.; Facchetti, A.; Lefenfeld, M.; Katz, H. E.; Marks, T. J. Easily Processable Phenylene–Thiophene-Based Organic Field-Effect Transistors and Solution-Fabricated Nonvolatile Transistor Memory Elements. *J. Am. Chem. Soc.* **2003**, *125*, 9414–9423.

(17) Kaltenbrunner, M.; Stadler, P.; Schwödiauer, R.; Hassel, A. W.; Sariciftci, N. S.; Bauer, S. Anodized Aluminum Oxide Thin Films for Room-Temperature-Processed, Flexible, Low-Voltage Organic Non-Volatile Memory Elements with Excellent Charge Retention. *Adv. Mater.* **2011**, *23*, 4892–4896.

(18) Tseng, C.-W.; Huang, D.-C.; Tao, Y.-T. Organic Transistor Memory with a Charge Storage Molecular Double-Floating-Gate Monolayer. *ACS Appl. Mater. Interfaces* **2015**, *7*, 9767–9775.

(19) Han, S. T.; Zhou, Y.; Xu, Z. X.; Huang, L. B.; Yang, X. B.; Roy, V. A. L. Microcontact Printing of Ultrahigh Density Gold Nanoparticle Monolayer for Flexible Flash Memories. *Adv. Mater.* **2012**, *24*, 3556–3561.

(20) Han, S. T.; Zhou, Y.; Wang, C.; He, L.; Zhang, W.; Roy, V. A. L. Layer-by-Layer-Assembled Recuced Graphene Oxide/Gold Nanoparticle Hybrid Double-Floating-Gate Structure for Low-Voltage Flexible Flash Memory. *Adv. Mater.* **2013**, *25*, 872–877.

(21) Park, Y. S.; Lee, J. S. Design of an Efficient Charge-Trapping Layer with a Built-in Tunnel Barrier for Reliable Organic-Transistor Memory. *Adv. Mater.* **2015**, *27*, 706–711.

DOI: 10.1021/acsnano.5b05313
ACS Nano 2016, 10, 436–445

(22) Tseng, C. W.; Tao, Y.-T. Electric Bistability in Pentacene Film-Based Transistor Embedding Gold Nanoparticles. *J. Am. Chem. Soc.* **2009**, *131*, 12441−12450.
(23) Burkhardt, M.; Jedaa, A.; Novak, M.; Ebel, A.; Voïtchovsky, K.; Stellacci, F.; Hirsch, A.; Halik, M. Concept of a Molecular Charge Storage Dielectric Layer for Organic Thin-Film Memory Transistors. *Adv. Mater.* **2010**, *22*, 2525−2528.
(24) Chang, M. F.; Lee, P. T.; McAlister, S. P.; Chin, A. A Flexible Organic Pentacene Nonvolatile Memory Based on High-*k* Dielectric Layers. *Appl. Phys. Lett.* **2008**, *93*, 023310.
(25) Zhou, Y.; Han, S.-T.; Chen, X.; Wang, F.; Tang, Y. B.; Roy, V. A. L. An Upconverted Photonic Nonvolatile Memory. *Nat. Commun.* **2014**, *5*, 4720.
(26) Orgiu, E.; Samorì, P. Organic Electronics Marries Photochromism: Generation of Multifunctional Interfaces, Materials, and Devices. *Adv. Mater.* **2014**, *26*, 1827−1845.
(27) Tsujioka, T.; Irie, M. Electrical Functions of Photochromic Molecules. *J. Photochem. Photobiol., C* **2010**, *11*, 1−14.
(28) Shen, Q.; Wang, L.; Liu, S.; Cao, Y.; Gan, L.; Guo, X.; Steigerwald, M. L.; Shuai, Z.; Liu, Z.; Nuckolls, C. Photoactive Gate Dielectrics. *Adv. Mater.* **2010**, *22*, 3282−3287.
(29) Li, Y.; Zhang, H.; Qi, C.; Guo, X. Light-Driven Photochromism-Induced Reversible Switching in P3HT-Spiropyran Hybrid Transistors. *J. Mater. Chem.* **2012**, *22*, 4261−4265.
(30) Zhang, H.; Guo, X.; Hui, J.; Hu, S.; Xu, W.; Zhu, D. Interface Engineering of Semiconductor/Dielectric Heterojunctions toward Functional Organic Thin-Film Transistors. *Nano Lett.* **2011**, *11*, 4939−4946.
(31) Raimondo, C.; Crivillers, N.; Reinders, F.; Sander, F.; Mayor, M.; Samorì, P. Optically Switchable Organic Field-Effect Transistors Based on Photoresponsive Gold Nanoparticles Blended with Poly(3-Hexylthiophene). *Proc. Natl. Acad. Sci. U. S. A.* **2012**, *109*, 12375−12380.
(32) Crivillers, N.; Orgiu, E.; Reinders, F.; Mayor, M.; Samorì, P. Optical Modulation of the Charge Injection in an Organic Field-Effect Transistor Based on Photochromic Self-Assembled-Monolayer-Functionalized Electrodes. *Adv. Mater.* **2011**, *23*, 1447−1452.
(33) Orgiu, E.; Crivillers, N.; Herder, M.; Grubert, L.; Pätzel, M.; Frisch, J.; Pavlica, E.; Duong, D. T.; Bratina, G.; Salleo, A.; et al. Optically Switchable Transistor *via* Energy-Level Phototuning in a Bicomponent Organic Semiconductor. *Nat. Chem.* **2012**, *4*, 675−679.
(34) Gemayel, M. E.; Börjesson, K.; Herder, M.; Duong, D. T.; Hutchison, J. A.; Ruzié, C.; Schweicher, G.; Salleo, A.; Geerts, Y.; Hecht, S.; et al. Optically Switchable Transistors by Simple Incorporation of Photochromic Systems into Small-Molecule Semiconducting Matrices. *Nat. Commun.* **2015**, *6*, 6330.
(35) Tseng, C.-W.; Huang, D.-C.; Tao, Y.-T. Electric Bistability Induced by Incorporating Self-Assembled Monolayers/aggregated Clusters of Azobenzene Derivatives in Pentacene-Based Thin-Film Transistors. *ACS Appl. Mater. Interfaces* **2012**, *4*, 5483−5491.
(36) Shallcross, R. C.; Körner, P. O.; Maibach, E.; Köhnen, A.; Meerholz, K. A Photochromic Diode with a Continuum of Intermediate States: Towards High Density Multilevel Storage. *Adv. Mater.* **2013**, *25*, 4807−4813.
(37) Jakobsson, F. L. E.; Marsal, P.; Braun, S.; Fahlman, M.; Berggren, M.; Cornil, J.; Crispin, X. Tuning the Energy Levels of Photochromic Diarylethene Compounds for Opto-Electronic Switch Devices. *J. Phys. Chem. C* **2009**, *113*, 18396−18405.
(38) Dulić, D.; van der Molen, S. J.; Kudernac, T.; Jonkman, H. T.; de Jong, J. J. D.; Bowden, T. N.; van Esch, J.; Feringa, B. L.; van Wees, B. J. One-Way Optoelectronic Switching of Photochromic Molecules on Gold. *Phys. Rev. Lett.* **2003**, *91*, 207402.
(39) Whalley, A. C.; Steigerwald, M. L.; Guo, X.; Nuckolls, C. Reversible Switching in Molecular Electronic Devices. *J. Am. Chem. Soc.* **2007**, *129*, 12590−12591.
(40) Jia, C.; Wang, J.; Yao, C.; Cao, Y.; Zhong, Y.; Liu, Z. R.; Liu, Z. F.; Guo, X. Conductance Switching and Mechanisms in Single-Molecule Junctions. *Angew. Chem., Int. Ed.* **2013**, *52*, 8666−8670.
(41) Acton, O.; Ting, G.; Ma, H.; Ka, J. W.; Yip, H.-L.; Tucker, N. M.; Jen, A. K.-Y. π-σ-Phosphonic Acid Organic Monolayer/Sol-Gel Hafnium Oxide Hybrid Dielectrics for Low-Voltage Organic Transistors. *Adv. Mater.* **2008**, *20*, 3697.
(42) Zhang, B.; Kong, T.; Xu, W.; Su, R.; Gao, Y.; Cheng, G. Surface Functionalization of Zinc Oxide by Carboxyalkylphosphonic Acid Self-Assembled Monolayers. *Langmuir* **2010**, *26*, 4514−4522.
(43) Katsonis, N.; Kudernac, T.; Walko, M.; van der Molen, S. J.; van Wees, B. J.; Feringa, B. L. Reversible Conductance Switching of Single Diarylethenes on a Gold Surfaces. *Adv. Mater.* **2006**, *18*, 1397−1400.
(44) Kronemeijer, A. J.; Akkerman, H. B.; Kudernac, T.; van Wees, B. J.; Feringa, B. L.; Blom, P. W. M.; de Boer, B. Reversible Conductance Switching in Molecular Devices. *Adv. Mater.* **2008**, *20*, 1467−1473.
(45) Kim, D.; Jeong, H.; Lee, H.; Hwang, W.-T.; Wolf, J.; Scheer, E.; Huhn, T.; Jeong, H.; Lee, T. Flexible Molecular-Scale Electronic Devices Composed of Diarylethene Photoswitching Molecules. *Adv. Mater.* **2014**, *26*, 3968−3973.
(46) Lemmetyinen, H.; Tkachenko, N. V.; Efimov, A.; Niemi, M. Photoinduced Intra- and Intermolecular Electron Transfer in Solutions and in Solid Organized Molecular Assemblies. *Phys. Chem. Chem. Phys.* **2011**, *13*, 397−412.
(47) She, C.; Guo, J.; Irle, S.; Morokuma, K.; Mohler, D. L.; Zabri, H.; Odobel, F.; Youm, K.-T.; Liu, F.; Hupp, J. T.; et al. Comparison of Interfacial Electron Transfer through Carboxylate and Phosphonate Anchoring Groups. *J. Phys. Chem. A* **2007**, *111*, 6832−6842.
(48) Bez, R.; Camerlenghi, E.; Modelli, A.; Visconti, A. Introduction to Flash Memory. *Proc. IEEE* **2003**, *91*, 489−502.
(49) Kim, T.-W.; Zeigler, D. F.; Acton, O.; Yip, H.-L.; Ma, H.; Jen, A. K.-Y. All-Organic Photopatterned One Diode-One Resistor Cell Array for Advanced Organic Nonvolatile Memory Applications. *Adv. Mater.* **2012**, *24*, 828−833.
(50) Nau, S.; Wolf, C.; Sax, S.; List-Kratochvil, E. J. W. Organic Non-Volatile Resistive Photo Switches for Flexible Image Detector Arrays. *Adv. Mater.* **2015**, *27*, 1048−1052.
(51) Acton, O.; Osaka, I.; Ting, G.; Hutchins, D.; Ma, H.; McCullough, R. D.; Jen, A. K.-Y. Phosphonic Acid Self-Assembled Monolayer and Amorphous Hafnium Oxide Hybrid Dielectric for High Performance Polymer Thin Film Transistors on Plastic Substrates. *Appl. Phys. Lett.* **2009**, *95*, 113305.
(52) Yoo, Y. B.; Park, J. H.; Lee, K. H.; Lee, H. W.; Song, K. M.; Lee, S. J.; Baik, H. K. Solution-Processed High-*k* HfO_2 Gate Dielectric Processed under Softening Temperature of Polymer Substrates. *J. Mater. Chem. C* **2013**, *1*, 1651−1658.

DOI: 10.1021/acsnano.5b05313
ACS Nano 2016, 10, 436−445